CuO-doped $NaNbO_3$ antiferroelectrics: Impact of aliovalent doping and nonstoichiometry on the defect structure and formation of secondary phases

Ebru Erünal,[1] Peter Jakes,[1] Sabine Körbel,[2] Jérôme Acker,[3] Hans Kungl,[3] Christian Elsässer,[2] Michael J. Hoffmann,[3] and Rüdiger-A. Eichel[1,*]

[1]*Institut für Physikalische Chemie, Universität Freiburg, Albertstr. 21, D-79104 Freiburg, Germany*

[2]*Fraunhofer-Institut für Werkstoffmechanik IWM, Wöhlerstr. 11, D-79108 Freiburg, Germany*

[3]*Institut für Angewandte Materialien–Keramik im Maschinenbau, Karlsruher Institut für Technologie, D-76131 Karlsruhe, Germany*

(Received 13 September 2011; published 28 November 2011)

The interplay between aliovalent CuO doping and nonstoichiometry on the development of defect structures and the formation of secondary phases of antiferroelectric $NaNbO_3$ ceramics has been investigated by means of x-ray diffraction (XRD), first-principles calculations using density functional theory (DFT), and electron paramagnetic resonance spectroscopy. The results indicate that, for stoichiometric 0.25 mol% CuO-doped $NaNbO_3$, as well as for 2.0 mol% Nb-excess sodium niobate, the Cu^{2+} functional centers are incorporated at the Nb site (Cu'''_{Nb}). For reasons of charge compensation, two kinds of mutually compensating defect complexes ($Cu'''_{Nb} - V_O^{\bullet\bullet})'$ and ($V_O^{\bullet\bullet} - Cu'''_{Nb} - V_O^{\bullet\bullet})^{\bullet}$ are formed where, for the niobium-excess compound, additionally, V'_{Na} contribute to the mechanism of charge compensation. In contrast, for 2.0 mol% Na-excess sodium niobate, a Na_3NbO_4 secondary phase has been detected by XRD, and only part of the Cu^{2+} forms these types of defect complexes. The major part of the Cu^{2+} is incorporated in a fundamentally different way by forming Cu^{2+}-Cu^{2+} dimeric defect complexes.

DOI: 10.1103/PhysRevB.84.184113 PACS number(s): 61.72.J−, 61.72.Bb, 85.50.−n

I. INTRODUCTION

Sodium niobate ($NaNbO_3$) is an antiferroelectric nonpolar material that transforms into a ferroelectric polar state when subjected to an external field of suitable strength.[1,2] Upon variation of temperature, $NaNbO_3$ exhibits an unusually large number of phase transitions, owing to tilted oxygen octahedra and off-centered Nb ions, rendering it one of the most complicated perovskite materials from a structural point of view.[1–3]

Materials from the $[K_{1-y}Na_y]NbO_3$ (KNN) solid-solution system and their modifications currently receive extensive interest for the development of lead-free ferroelectrics.[4–7] Modification of these materials by CuO or Cu-containing sintering additives is one line of development to improve these groups of materials.[8–13] Accordingly, two effects from aliovalent Cu doping may influence the materials properties: (i) changes in the defect structure by formation of lattice vacancies and defect complexes[14–17] and (ii) the presence of secondary phases forming during sintering, which may be favored in cases when nonstoichiometry of the alkaline niobate composition promotes their formation or when the solubility limit for the dopant is exceeded.[17,18] Here, we report on an analysis of the interplay of nonstoichiometry and aliovalent doping on the development of defect structure and the formation of secondary phase in CuO-doped $NaNbO_3$, one of the end members of the KNN system, by using electron paramagnetic resonance (EPR) spectroscopy[19] and density functional theory (DFT) calculations.[14,20]

II. EXPERIMENT

A. Materials

Sodium niobate powders doped with 0.25 mol% Cu were prepared by a solid-state route from high-purity Na_2CO_3, Nb_2O_5, and CuO raw materials.[18] Batch compositions with three different stoichiometries were prepared: $Na_{1.02}(Nb_{0.9975}Cu_{0.0025})O_3$, $Na(Nb_{0.9975}Cu_{0.0025})O_3$, and $Na_{0.98}(Nb_{0.9975}Cu_{0.0025})O_3$, corresponding to 2 mol% *A*-site excess, stoichiometric, and 2 mol% *B*-site excess materials in case of *B*-site substitution of Cu.

The materials were sintered at 1105 °C for 2 h in air. X-ray diffraction (XRD) patterns recorded in a Siemens D500 Diffractometer with Cu-K_α ($\lambda = 1.5406$ Å) radiation confirmed the formation of sodium niobate corresponding to JCPDS powder diffraction file 33-1270. While no reflections apart from those attributed to sodium niobate were identified in the diffraction patterns of the stoichiometric and the *B*-site excess sodium niobate materials, in the $Na_{1.02}(Nb_{0.9975}Cu_{0.0025})O_3$ composition, additional small peaks with intensities two orders of magnitude lower than for the sodium niobate reflections were detected, indicating the presence of a secondary phase in the ceramics with *A*-site excess.

Depending on stoichiometry of the $NaNbO_3$-Cu ceramics, different types of microstructure develop. In the *A*-site excess composition, $Na_{1.02}(Nb_{0.9975}Cu_{0.0025})O_3$ grains grow to approximately 10 to 40 μm with cuboid forms and plane surfaces [cf. Fig. 1(a)]. The stoichiometric $Na(Nb_{0.9975}Cu_{0.0025})O_3$ ceramic consists of very large, 100 to 500 μm sized, nonpolyhedral-shaped grains with considerable intragranular porosity [cf. Fig. 1(b)]. In the ceramics with *B*-site excess, the microstructure is fine grained with grain size between 5 and 10 μm [cf. Fig. 1(c)]. These microstructural features correspond to the stoichiometry-dependent characteristics reported for undoped *A*-site excess, stoichiometric, and *B*-site excess sodium-potassium niobate.[18]

B. EPR spectroscopy

To characterize the defect structure, EPR experiments were performed on an *X*-band (9.5-GHz) EPR spectrometer (Bruker, EMX) in a temperature interval ranging between 10 and 300 K, using a helium-flow cryostat (Oxford). For the exact calibration of the magnetic field, a NMR gaussmeter

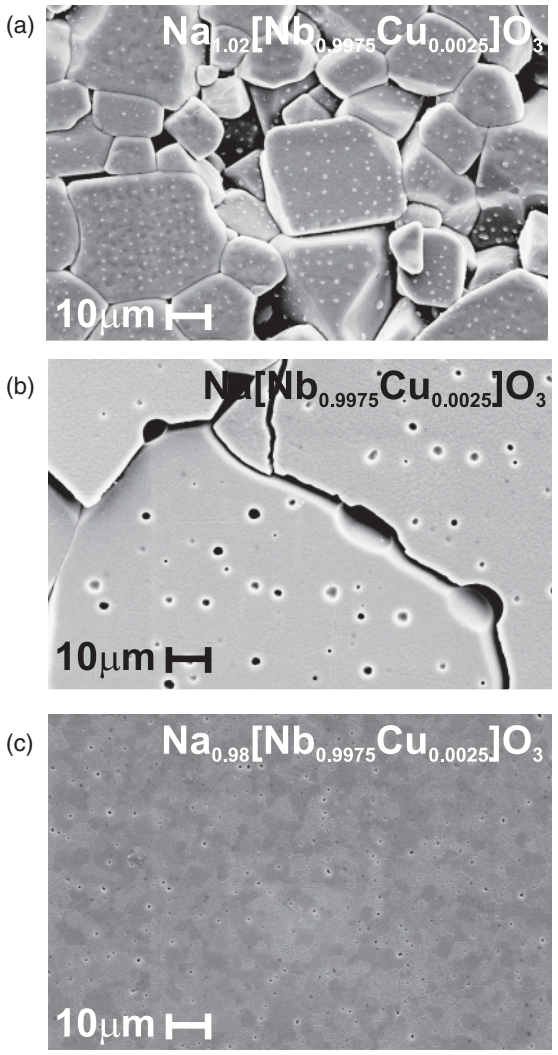

FIG. 1. Microstructure of 0.25 mol% $NaNbO_3$ ceramics of varying Na/Nb stoichiometries, sintered at 1105 °C for 2 h and chemically etched after polishing. (a) 2.0 mol% Na-excess $Na_{1.02}[Nb_{0.9975}Cu_{0.0025}]O_3$. (b) Stoichiometric $Na[Nb_{0.9975}Cu_{0.0025}]O_3$. (c) 2.0 mol% Nb-excess $Na_{0.98}[Nb_{0.9975}Cu_{0.0025}]O_3$.

(ER 035M, Bruker) and a standard field marker polycrystalline DPPH with $g = 2.0036$ were used.

III. THEORY

A. Density functional theory calculations

First-principles calculations using density functional theory (DFT) in the local-density approximation (LDA) were performed to determine the thermodynamically most stable lattice site for isolated Cu substitutionals in $NaNbO_3$ by comparing defect formation enthalpies for the substitution on Na and Nb sites:

$$E^f[X^q] = E_{\text{tot}}[X^q] - E_{\text{tot}}[\text{bulk}] - \sum_i \mu_i n_i + q \cdot E_F,$$

where $E^f[X^q]$ is the total energy of a defect X with defect charge q, $E_{\text{tot}}[\text{bulk}]$ is the energy of a perfect reference cell, n_i is the number of atoms of species i exchanged with a reservoir, μ_i is its chemical potential, and E_F is the chemical potential of the electrons (the Fermi energy).

The chemical potentials are approximated by total energies per atom in the crystalline solids; for the oxygen gas, a temperature and pressure correction based on the ideal gas equation is made. This approach is described in detail in a review article of Van de Walle and Neugebauer[21] and in Ref. 22. It was applied to the KNN system in Refs. 23 and 14. The chemical potential of the electrons is treated as a variable that is allowed to vary over the band gap of $NaNbO_3$. The theoretical band-gap energy of 1.80 eV obtained with the LDA is used. Although the LDA underestimates the band gap severely, in a similar study of KNN, we found that the predicted substitution site of Cu dopants is the same, whether a band-gap correction is applied or not.

The total energies of perfect and defect structures were calculated with the mixed-basis pseudopotential (MBPP) code[24–28] using a basis of plane waves up to 340 eV combined with atom-centered functions for Na $s + p$ semicore states, O p valence states, Nb $s + p$ semicore and d valence states, and Cu d valence states. The atoms were represented by optimally smooth norm-conserving pseudopotentials as proposed in Ref. 29.

The LDA exchange-correlation functional as parametrized by Perdew and Zunger[30] was used. Simple cubic $2 \times 2 \times 2$ supercells and k meshes that correspond to an $8 \times 8 \times 8$ Monkhorst-Pack mesh in the single perovskite unit cell and Gaussian broadening by 0.2 eV were employed. The atomic positions were relaxed until the forces were smaller than 10 meV/Å.

B. EPR spin Hamiltonian

The spin Hamiltonian for a magnetically dilute Cu^{2+} center ($3d^9$) with electron spin $S = \frac{1}{2}$ (*monomeric* Cu^{2+}) can be written as[31]

$$\mathcal{H}_{S=\frac{1}{2}} = \beta_e \mathbf{B_0} \cdot \mathbf{g} \cdot \mathbf{S} - \beta_n g_n \mathbf{B_0} \cdot \mathbf{I} + \mathbf{S} \cdot \mathbf{A} \cdot \mathbf{I}, \qquad (1)$$

where g_n is the corresponding nuclear g factor and β_e and β_n are the Bohr and nuclear magnetons, respectively. The first and second terms represent the electronic and nuclear Zeeman interactions, respectively, where $\mathbf{B_0}$ denotes the external field, given in the principal axes system of the $\mathbf{g}$ matrix. The third term is due to the copper hyperfine interaction with $I^{\text{Cu}} = \frac{3}{2}$ for both copper isotopes with natural abundances ^{63}Cu:69.09% and ^{65}Cu:30.91%.

On the other hand, the spin-pair Hamiltonian describing the interaction between two Cu^{2+} centers with local electron spin $S_1 = S_2 = \frac{1}{2}$ and total electron triplet state $S = 1$ (*dimeric* Cu^{2+}) has to consider additional terms, such that the corresponding spin Hamiltonian is written as[32,33]

$$\mathcal{H}_{S=1} = \beta_e \sum_{i=1}^{2} \mathbf{B_0} \cdot \mathbf{g} \cdot \mathbf{S}_i - \beta_n g_n \mathbf{B_0} \cdot \mathbf{I} + \sum_{i=1}^{2} \mathbf{S} \cdot \mathbf{A} \cdot \mathbf{I}_i - J\mathbf{S_1} \cdot \mathbf{S_2} + \mathbf{S_1} \cdot \mathbf{D} \cdot \mathbf{S_2}. \qquad (2)$$

The last two terms describe the isotropic Heisenberg and the anisotropic dipolar spin-exchange interactions, respectively. In that notation, J is the isotropic exchange constant and $\mathbf{D}$ is the fine-structure tensor that combines

contributions from anisotropic exchange interaction (D_{ex}) and magnetic dipole-dipole interactions (D_{dd}). The fine-structure interaction is commonly parametrized in terms of the sum $\sum_{k=2,\ldots,2S}^{-q\leqslant k\leqslant q} B_k^q O_k^q(S_x,S_y,S_z)$, with B_k^q the fine-structure Hamiltonian coefficients and O_k^q the extended Stevens spin operators.[31] The order k in the spin operators for two magnetically coupled centers of $S = 1$ allows terms up to $k = 2$. $\mathbf{S_{1,2}}$ and $\mathbf{I_{1,2}}$ are the spin operators of the individual components of the dimer.

Adopting a point-dipole approximation, D_{dd} allows us to estimate the distance r_{12} between the two Cu^{2+} centers according to

$$D_{dd} = \frac{3}{4}\frac{g_\parallel^2\beta^2(1-3\cos^2\theta)}{r_{12}^3}, \qquad (3)$$

where θ is the angle between the direction of r_{12} and the external magnetic field.

IV. RESULTS AND DISCUSSION

The X-band (9.5-GHz) EPR spectra of 0.25 mol% CuO-modified $NaNbO_3$ for varying Na/Nb stoichiometries are shown in Fig. 2. The compounds with 2.0 mol% Nb-excess ($Na_{0.98}[Nb_{0.9975}Cu_{0.0025}]O_3$) and stoichiometric $Na[Nb_{0.9975}Cu_{0.0025}]O_3$ show characteristic spectral features for an $S = \frac{1}{2}$ system with quartet hyperfine coupling to a nucleus of $I = \frac{3}{2}$. This is indicative for the Cu^{2+}-oxidation state with $3d^9$.[31,32] Particularly at low temperature (20 K), two different sets of quartet hyperfine resonances (A_{zz}) can be distinguished in the low-field region, centered at slightly different g values (g_{zz}). The origin for such differences in hyperfine patterns can be explained by Cu^{2+} centers with varying oxygen coordination, i.e., defect complexation with charge-compensating oxygen vacancies.[34]

With respect to the temperature dependence, sodium niobate is known to exhibit a phase transition at 193 K from the antiferroelectric, monoclinic phase at ambient temperature to a ferroelectric, rhombohedral phase. This phase transition can also be monitored by the corresponding EPR spectra measured at ambient temperature [cf. Fig. 2(a)] as compared to those at 20 K [Fig. 2(b)] and tentatively can be traced back to the expected tilting of oxygen octahedra and off-centering of the B-site ions as a function of temperature.[1–3]

The spectra for the 2.0 mol% Na-excess compound ($Na_{1.02}[Nb_{0.9975}Cu_{0.0025}]O_3$), however, substantially differ from those typically obtained if the Cu^{2+} ions reside at the octahedrally coordinated sites in a magnetically dilute state.[15,16,35–41] Instead, the spectra are characteristic for a triplet ($S = 1$) state that may be explained by a Cu^{2+}-Cu^{2+} dimeric center owing to the here observed septet hyperfine pattern as compared to the quartet hyperfine pattern present for the other compounds.

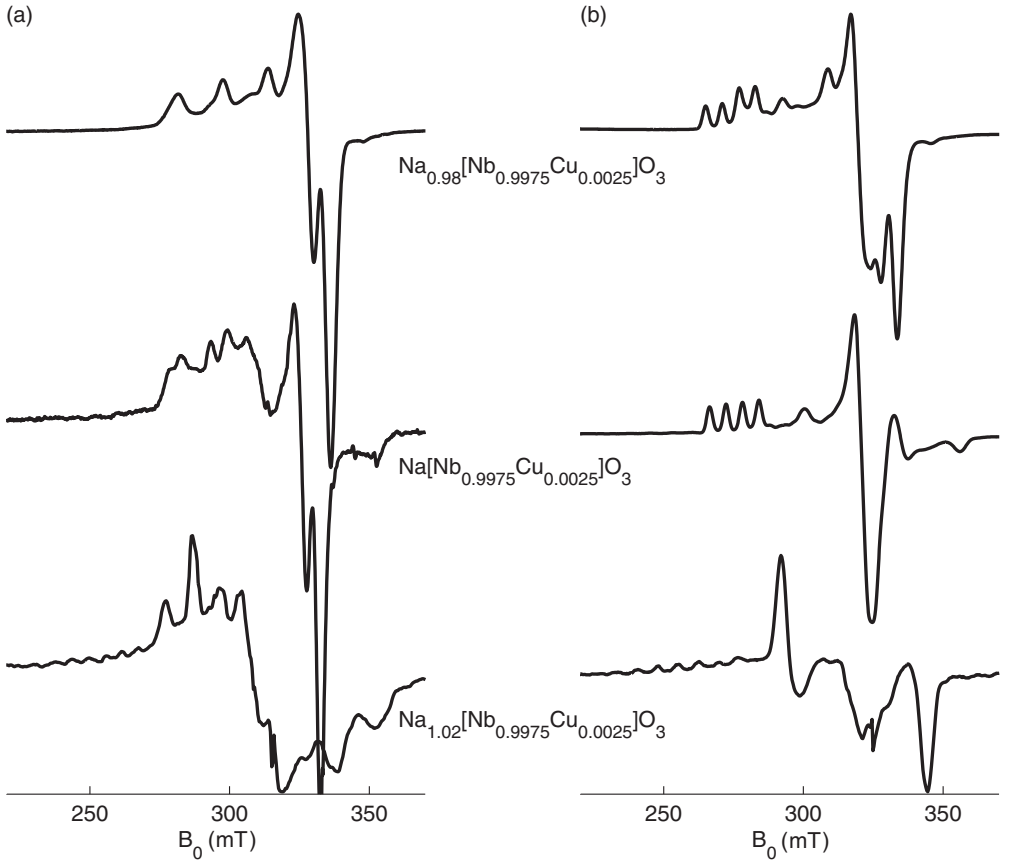

FIG. 2. X-band (9.5 GHz) EPR spectra of a 0.25 mol% CuO-doped $NaNbO_3$ ceramics measured at (a) ambient temperature and (b) at 20 K. 2.0 mol% Nb-excess ($Na_{0.98}[Nb_{0.9975}Cu_{0.0025}]O_3$, top), stoichiometric ($Na[Nb_{0.9975}Cu_{0.0025}]O_3$, center), and 2.0 mol% Na-excess ($Na_{1.02}[Nb_{0.9975}Cu_{0.0025}]O_3$, bottom) CuO-doped sodium niobate.

A. Stoichiometric Cu^{2+}:$NaNbO_3$

Principally, Cu^{2+} in alkali niobates is discussed being incorporated at both cation sites, where the Cu^{2+} either acts as an acceptor or a donor and charge compensation is performed by cation or anion vacancies.[42] Considering first the stoichiometric CuO-doped $NaNbO_3$, DFT calculations predict an incorporation of Cu on the Nb site under air atmosphere. The results are illustrated in the phase-stability diagram for Cu-doped $NaNbO_3$ in Fig. 3. The perovskite phase is stable for chemical potentials in the gray region, whereas outside that region, it becomes unstable with respect to competing oxide phases, such as Na_2O or Nb_2O_5. The substitution of Cu at the Na site is thermodynamically favorable for a low chemical potential of oxygen or partial pressures (light gray area marked as Cu_{Na} in Fig. 3), whereas for a high chemical potential of oxygen, corresponding to processing under air atmosphere at atmospheric pressure, the substitution of Cu at the Nb site is thermodynamically more stable, at least at room temperature (dark gray area marked as Cu_{Nb} in Fig. 3). In the intermediate gray-shaded area, the preferred substitution site depends on the position of the Fermi level in the band gap.

The prediction by DFT is supported by the EPR experiments, as the obtained spectra are characteristic for a situation for which $g_{zz} > g_{yy}, g_{xx}$. Accordingly, the Cu^{2+} site has to be octahedrally coordinated, which corresponds to the perovskite B site. The sizes of ionic radii, with $r_{Nb^{5+}} = 64$ pm and $r_{Cu^{2+}} = 73$ pm, as compared to $r_{Na^{+}} = 139$ pm, support this assignment.

For an analysis of defect structures, the overlapping Cu^{2+} EPR spectra were first unraveled by employing numerical spectrum simulation.[43] Correspondingly, the obtained spectrum for the stoichiometric $Na[Nb_{0.9975}Cu_{0.0025}]O_3$ compound is shown to consist of two subspectra as depicted in Fig. 4(a).

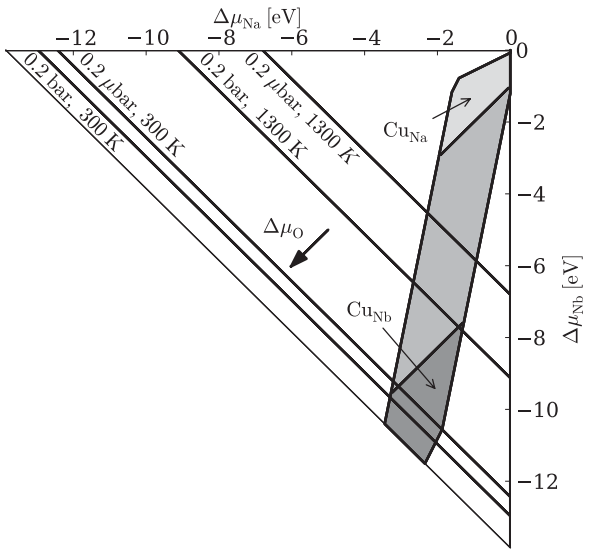

FIG. 3. Phase-stability diagram as obtained with DFT. The perovskite structure is stable for chemical potentials in the gray region. The oxygen chemical potentials corresponding to the standard atmospheric pressure and to 10^{-6} bar at temperatures of 300 K (room temperature) and at 1300 K (close to typical sintering temperatures), respectively, are indicated by black lines.

The refined spin-Hamiltonian parameters for the two Cu^{2+} centers are summarized in Table I.

In order to transfer the determined spin-Hamiltonian parameters into structural information, sets of g-value and ^{63}Cu-hyperfine coupling (g_{zz}, $^{63Cu}A_{zz}$) are analyzed owing to a recently developed semiempirical scheme.[34] The different defects are designated by using the Kröger-Vink notation,[44] according to which the subscript indicates the lattice site that a defect occupies and the superscript corresponds to the electronic charge of the defect relative to the site that it occupies. To indicate isovalent substitution charge, $\times$ is used, $\bullet$ indicates a single positive charge, and $'$ signifies negative charge. By exploiting refined spin-Hamiltonian pairs (g_{zz}, $^{Cu}A_{zz}$) for the two centers observed, the formation of two different kinds of charged defect complexes is confirmed: $(V_O^{\bullet\bullet} - Cu_{Nb}''' - V_O^{\bullet\bullet})^{\bullet}$ and $(Cu_{Nb}''' - V_O^{\bullet\bullet})'$. In the first complex $(V_O^{\bullet\bullet} - Cu_{Nb}''' - V_O^{\bullet\bullet})^{\bullet}$, Cu^{2+} is electrically overcompensated with two oxygen vacancies. Owing to the Jahn-Teller effect, we tentatively assign the two oxygen vacancies being coordinated at the two apical sites of the oxygen octahedron, such that the defect complex approximately is inversion symmetric (although the host compound is noninversion symmetric). This assignment is supported by the observed almost axial symmetry of the spin-Hamiltonian g matrix ($g_{xx} \approx g_{yy}$) and is in analogy to results recently found for similar compounds.[14–16] In a linearly aligned defect complex, we expect that the Cu^{2+} ion relaxes into the plane spanned by the four equatorial oxygens in analogy to the situation reported for acceptor centers in other ferroelectric materials.[14,45–49] As a consequence, the distance to the oxygen vacancies is approximately equal, for which reason this defect complex contains a vanishing electric dipole moment. On the other hand, the two $V_O^{\bullet\bullet}$, as well as the Cu^{2+}, will deform the lattice, leading to an *elastic dipole* moment.[50]

The second complex $(Cu_{Nb}''' - V_O^{\bullet\bullet})'$ is electrically undercompensated by only one oxygen vacancy. Consequently, this defect complex contains an *electric dipole* moment $p_D = q \cdot l$ with $q = +2e$ at the oxygen vacancy site and $q = -3e$ at the Cu^{2+} site, both having a distance of about half a lattice constant.[51,52]

Concerning the overall charge compensation of the compound, the two kinds of defect complexes are singly charged, but with opposite signs. Hence, they can *mutually compen-*

TABLE I. Determined spin-Hamiltonian parameters for different Cu^{2+} functional centers in $NaNbO_3$ at a temperature of 20 K, as refined after numerical spectrum simulation. Within spectral resolution, $g_{xx} \approx g_{yy}$ and $A_{xx}^{Cu} \approx A_{yy}^{Cu}$. Diverging spin-Hamiltonian values for the Nb-excess compound are given in parentheses.

	$(V_O^{\bullet\bullet} - Cu_{Nb}''' - V_O^{\bullet\bullet})^{\bullet}$	$(Cu_{Nb}''' - V_O^{\bullet\bullet})'$	Cu^{2+}-Cu^{2+}
g_{zz}	2.235 (2.170)	2.450	2.235
g_{xx}	2.057 (2.092)	2.092	2.105
$^{63Cu}A_{zz}$	480 MHz (520 MHz)	205 MHz	230 MHz
$^{63Cu}A_{xx}$	40 MHz	40 MHz	50 MHz
B_2^0			430 MHz

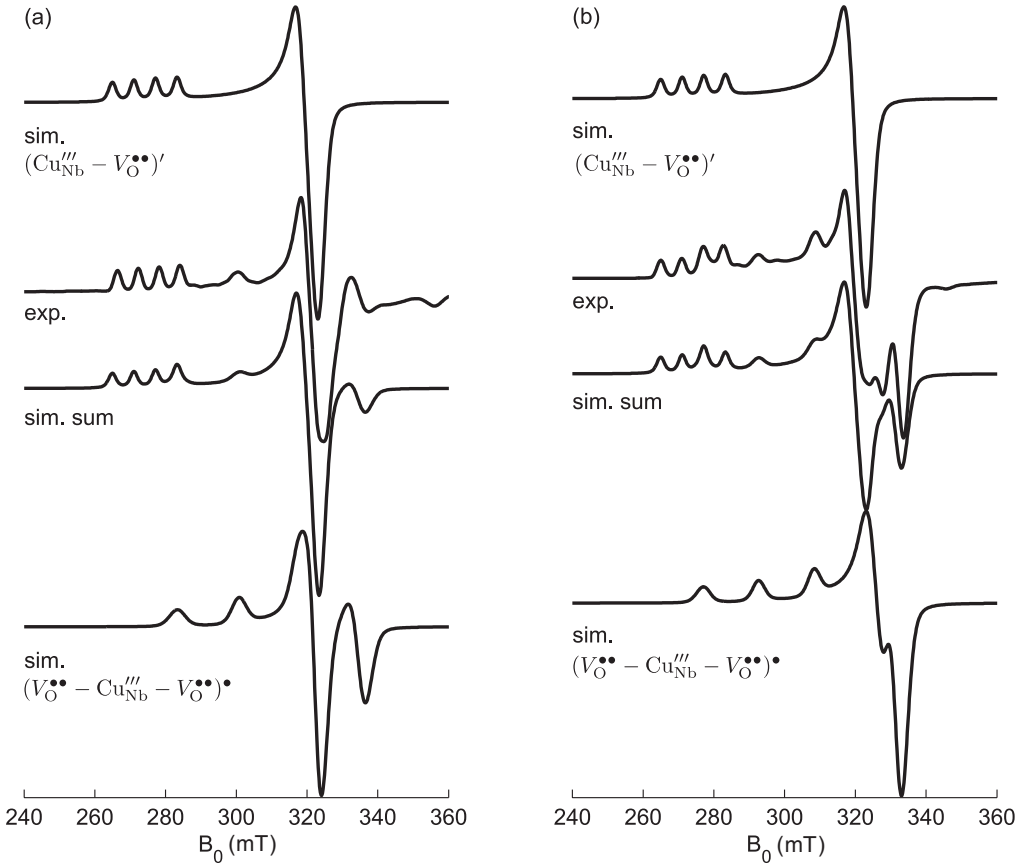

FIG. 4. Deconvolution of overlapping Cu^{2+} species for stoichiometric (a) and 2.0 mol% Nb-excess CuO-doped $NaNbO_3$ (b). Experimental *X*-band (9.5-GHz) EPR spectra (center) measured at 20 K compared to numerical spectrum simulations (top, center) invoking the spin-Hamiltonian parameters given in Table I for the $(Cu'''_{Nb} - V_O^{\bullet\bullet})'$ and $(V_O^{\bullet\bullet} - Cu'''_{Nb} - V_O^{\bullet\bullet})^{\bullet}$ defect complexes. The numerically simulated sum spectrum is a superposition of both subspectra.

sate according to the following approximation for charge neutrality:

$$[(Cu'''_{Nb} - V_O^{\bullet\bullet})'] \approx [(V_O^{\bullet\bullet} - Cu'''_{Nb} - V_O^{\bullet\bullet})^{\bullet}]. \quad (4)$$

This is in line with the observation that both defect centers are approximately equally abundant for the stoichiometric 0.25 mol% Cu-doped sodium niobate compound. The amount of intrinsically present lattice defects V'_{Na} and $V_O^{\bullet\bullet}$ is thus not affected by the aliovalent Cu^{2+} doping.

The incorporation reaction of Cu^{2+} into the $NaNbO_3$ lattice is analogous to the situation for CuO-doped KNN 50/50 (Ref. 15) and $KNbO_3$ (Ref. 16):

$$2CuO \xrightarrow{Nb_2O_5} 2Cu'''_{Nb} + 2O_O^{\times} + 3V_O^{\bullet\bullet}, \quad (5)$$

which involves that each copper functional center in average is charge compensated by $\frac{3}{2}V_O^{\bullet\bullet}$. At the *high-temperature limit* valid for calcination and sintering, these $V_O^{\bullet\bullet}$ will be remote from the Cu^{2+} defect and, thus, are mobile ionic charge carriers. However, at the *low-temperature limit* valid well below the Curie temperature, the additionally introduced $V_O^{\bullet\bullet}$ to the $NaNbO_3$ lattice are trapped by the Cu^{2+} functional centers and form defect complexes according to

$$2Cu'''_{Nb} + 3V_O^{\bullet\bullet} \longrightarrow (Cu'''_{Nb} - V_O^{\bullet\bullet})' + (V_O^{\bullet\bullet} - Cu'''_{Nb} - V_O^{\bullet\bullet})^{\bullet}. \quad (6)$$

As compared to the situation for CuO-doped PZT materials, where only the fully charge-compensated $(Cu''_{Zr,Ti} - V_O^{\bullet\bullet})^{\times}$ defect dipole is present,[40,49] the defect structure present here is considerably more complicated. The reason is the pentavalent *B* site in $NaNbO_3$ as compared to the tetravalent one in PZT, such that a single $V_O^{\bullet\bullet}$ is not sufficient to compensate a Cu'''_{Nb} functional center.

B. Nb-excess Cu^{2+}:$NaNbO_3$

Generally, when considering the defect chemistry of ABO_3 materials with two different kinds of cation vacancies (V'_{Na}, V''''''_{Nb}), in principle, have to be accounted for. For the undoped $NaNbO_3$ compound, these cation vacancies are charge compensated by the corresponding anion vacancies ($V_O^{\bullet\bullet}$) according to the following approximation of charge neutrality:[17]

$$[V'_{Na}] + 5[V''''''_{Nb}] \approx 2[V_O^{\bullet\bullet}]. \quad (7)$$

Assuming that nonstoichiometry of a compound mainly impacts the concentration of cation vacancies, for Nb-excess $NaNbO_3$, the amount of V''''''_{Nb} is expected to be decreased, whereas for Na-excess $NaNbO_3$, the concentration of V'_{Na} is reduced. Vice versa, assuming the amount of unbound $[V_O^{\bullet\bullet}]$ to remain constant, because the additionally introduced oxygen

vacancies are complexed to the copper according to Eq. (6), Eq. (7) predicts that, with decreasing $[V_{Nb}^{'''''}]$, $[V_{Na}^{'}]$ should be increased.

The results obtained for the stoichiometric compound can be essentially transferred to the 2.0 mol% Nb-excess compound, as there were only minor differences in the refined spin-Hamiltonain parameters (cf. Table I). The main difference is the modified ratio of the amounts of the two defect centers because $[(Cu_{Nb}^{'''} - V_O^{\bullet\bullet})']$ is decreased as compared to $[(V_O^{\bullet\bullet} - Cu_{Nb}^{'''} - V_O^{\bullet\bullet})^{\bullet}]$. This can be explained by an increased amount of $[V_{Na}^{'}]$ present in the Nb-excess compound, which is in accordance to the prediction of Eq. (7) made for Nb-excess $NaNbO_3$. Correspondingly, the approximation for charge neutrality for the Nb-excess compound has to be modified as compared to the stoichiometric compound given in Eq. (4) according to

$$[V_{Na}^{'}] + [(Cu_{Nb}^{'''} - V_O^{\bullet\bullet})'] \approx [(V_O^{\bullet\bullet} - Cu_{Nb}^{'''} - V_O^{\bullet\bullet})^{\bullet}]. \quad (8)$$

Tentatively, the small variance in spin-Hamiltonian parameters for the $(V_O^{\bullet\bullet} - Cu_{Nb}^{'''} - V_O^{\bullet\bullet})^{\bullet}$ defect complex in the stoichiometric compound as compared to Nb-excess Cu^{2+}:$NaNbO_3$ can be rationalized by $V_{Na}^{'}$ in close vicinity to the defect complex.

Secondary phases were not observed, neither in the XRD nor in the EPR spectra (cf. Fig. 2), which is in line with a recent study of undoped sodium niobate, where it was reported that the material can tolerate niobium excess up to 4 mol% before secondary phases are formed.[53]

C. Na-excess Cu^{2+}:$NaNbO_3$

Considering Eq. (7) for a Na-excess $NaNbO_3$ compound, a reduced amount of $V_{Na}^{'}$ and simultaneously an increased concentration of $V_{Nb}^{'''''}$ are expected. However, pentavalent $V_{Nb}^{'''''}$ are generally regarded as quite improbable to exist owing to their high effective charge, which corresponds to a major disruption of the chemical bonding in the lattice. This is in line with recent DFT calculations that reported the energy of formation for sodium and oxygen vacancies being considerably lower as compared to the energy for a niobium vacancy.[54] Correspondingly, in analogy to considerations for nonstoichiometric $BaTiO_3$,[55] the contribution of $V_{Nb}^{'''''}$ to the defect equilibria is neglected and the formation of a NaO-rich secondary phase is expected until a stoichiometric $NaNbO_3$ compound is achieved.[17] In the case of Na-excess Cu^{2+}-doped $NaNbO_3$, the secondary phase likely contains copper as well.

As compared to the 2.0 mol% Nb-excess and stoichiometric CuO-doped $NaNbO_3$ compounds, the spectrum for the 2.0 mol% Na-excess compound ($Na_{1.02}[Nb_{0.9975}Cu_{0.0025}]O_3$) exhibits an additional spectral feature, which is characteristic for a triplet state with electron spin $S = 1$, as can be shown by numerical spectrum simulation (cf. Fig. 5).

The most striking difference to the spectra obtained for the above-discussed Nb-excess and stoichiometric sodium niobates is the well-resolved septet hyperfine splitting in the magnetic field range between 220 and 280 mT. As compared to the equally intense quartet hyperfine patterns characteristic for the other compositions (cf. Fig. 4), the septet hyperfine pattern can be explained by a hyperfine interaction to two magnetically equivalent copper nuclei, resulting in a

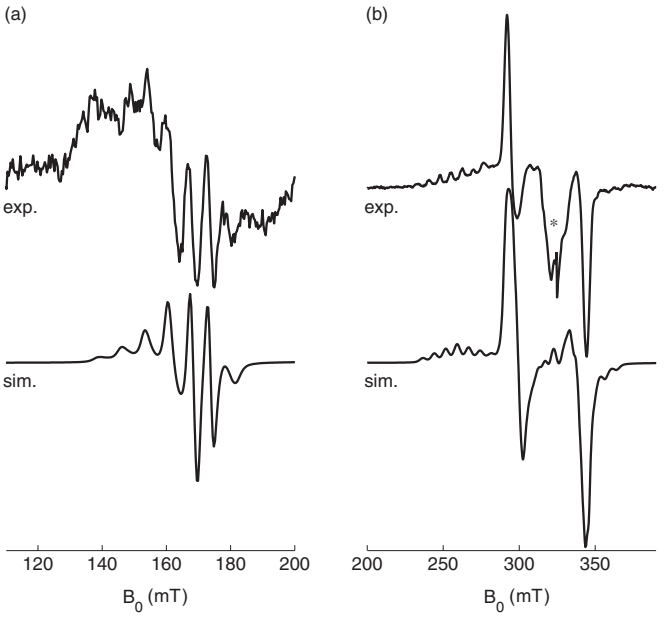

FIG. 5. Experimental X-band (9.5-GHz) EPR spectrum (top) of 2.0 mol% Na-excess CuO-doped $NaNbO_3$ measured at 20 K compared to a numerical spectrum simulation (bottom) invoking a triplet ($S = 1$) Cu^{2+}-Cu^{2+} dimeric center. The corresponding spin-Hamiltonian parameters are given in Table I. Forbidden *half-field* transitions with $\Delta m_S = \pm 2$ (a) and scaled intensity as compared to the allowed transitions with $\Delta m_S = \pm 1$ (b). The underlying resonance owing to the formation of defect complexes is indicated by an asterisk.

characteristic variation in intensity as 1 : 2 : 3 : 4 : 3 : 2 : 1. This situation is schematically illustrated in Fig. 6.

The resolved septet hyperfine interaction, however, is only resolved for the atomic z orientation; in the x and y orientations, the copper hyperfine interaction is too small to be resolved. The characteristic doublet resonance pattern observed in a field range between 290 and 350 mT is characteristic for the triplet ($S = 1$) electron spin state and

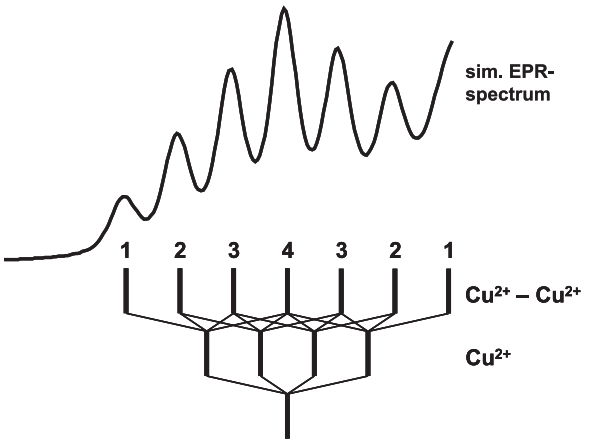

FIG. 6. Schematic illustration for the septet hyperfine splitting observed for the Cu^{2+}-Cu^{2+} dimeric center. The septet hyperfine pattern originates from a hyperfine interaction of two magnetically equivalent Cu^{2+} nuclei resulting in a characteristic variation in intensity as 1 : 2 : 3 : 4 : 3 : 2 : 1.

a situation for which $|J| \gg h\nu_{mw}$ holds. Consequently, the observed center has to involve a Cu^{2+}-Cu^{2+} dimer with dipolar spin-spin interaction, and transitions can only be induced within the spin-triplet state. By invoking the set of spin-Hamiltonian parameters summarized in Table I, this part of the experimental spectrum can be well reproduced numerically (cf. Fig. 5).

The resonance at 320 mT ($g = 2.108$) is not reproduced by the numerical spectrum simulation using the above-mentioned spin-Hamiltonian parameters of the Cu^{2+}-dimeric functional center. Owing to its g value, it can be assigned to the $g_{xx,yy}$ region of $(Cu'''_{Nb} - V_O^{\bullet\bullet})'$ and $(V_O^{\bullet\bullet} - Cu'''_{Nb} - V_O^{\bullet\bullet})^{\bullet}$ defect complexes.

A consequence of high-spin ($S = 1$) paramagnetic centers is that often resonances with considerably smaller intensity occur in a field range exactly at half the resonance field of the allowed transitions. These transitions at 140–180 mT are thus named as *half-field transitions*. Such resonances occur owing to so-termed *forbidden transitions* with selection rule $\Delta m_S = \pm 2$. Correspondingly, these transitions only occur for high-spin systems with electron spin ($S > \frac{1}{2}$). Because the half-field resonances additionally have a markedly smaller orientation dependence as compared to the *allowed transitions* with $\Delta m_S = \pm 1$, the corresponding resonances are typically better resolved and, thus, helpful signals for numerical spectrum simulation. The corresponding orientation dependence of allowed and forbidden transitions is depicted in Fig. 7.

By exploiting the calculated orientation dependence, it can be demonstrated that only the low-field septet hyperfine pattern for the g_{zz} orientation is observed in the EPR spectrum. This is owing to the g anisotropy, for which reason the high-field septet hyperfine resonances for the g_{zz} orientation are buried under the dipolar electron-spin doublet for the $g_{xx,yy}$ orientation.

For the observed Cu^{2+}-Cu^{2+} dimeric center, the distance between the two magnetically active copper sites can be estimated with two alternative methods. First, the determined fine-structure coupling B_2^0 can be analyzed according to the point-dipole approximation given in Eq. (3). Due to the similarity of the here obtained spectra with data from literature,[56–59] it can be assumed that $D_{dd} \gg D_{ex}$. Accordingly, D_{ex} is neglected and D_{dd} is taken as the dominant contribution to the fine-structure interaction, such that the numerically refined value of $B_2^0 = 430$ MHz can be used for the estimation of distance between the Cu^{2+} centers according to Eq. (3). Because, furthermore, the exact value for θ can only be obtained from single-crystal data, we tentatively set $\theta = 0$ as the Cu^{2+}-Cu^{2+} dimer most probably determines the orientation of the molecular frame with the main axis along the direction of r_{12}. Thus, with the determined value of $B_2^0 = 430$ MHz and taking $\theta = 0$, an interspin distance of $r_{12} = (3.3 \pm 0.5)$ Å is estimated. This value, however, is afflicted with a systematic error as the g values for the corresponding electron spins are assumed being isotropic and are approximated to $g = 2.0$, which differs to the here present g anisotropy (cf. Table I).

Second, the intensity of the *forbidden* half-field transition I_{HF} can be compared with the intensity of the *allowed* transition I, which obeys an r^{-6} law[60]

$$\frac{I_{HF}}{I} = \frac{(19.5 \pm 0.5)(9.1)^2}{r_{12}^6 \nu_{mw}^2}. \tag{9}$$

Here, ν_{mw} is the corresponding microwave frequency in GHz. Exploiting Eq. (9), the corresponding interspin distance can be estimated to $r_{12} = (2.9 \pm 0.5)$ Å. A major error occurs owing to the resonance at 320 mT ($g = 2.108$) that does not belong to the Cu^{2+}-Cu^{2+} dimer, but contributes to I. The hence determined value for r_{12} systematically overestimates the interspin distance.

As a mean value for the further considerations, we thus consider an interspin distance of (3.1 ± 0.5) Å between the two Cu^{2+} centers to discuss different conceivable defect-structure models. In that respect, three scenarios will be discussed: (i) an incorporation of the Cu^{2+}-Cu^{2+} dimer into the $NaNbO_3$ lattice, (ii) a magnetically dilute Cu^{2+}-Cu^{2+} dimer as impurity in a $Na_xNb_yO_z$ secondary phase, and (iii) strongly magnetically interacting Cu^{2+} centers as part of a $Na_xCu_yO_z$ secondary phase.

First, different processes of *self-complexation* are considered in which the two Cu^{2+} ions are assumed being incorporated in *linear* arrangements in neighboring unit cells of the $NaNbO_3$ structure, as schematically illustrated in Figs. 8(a)–8(c). In that respect, a substitution for the Na site

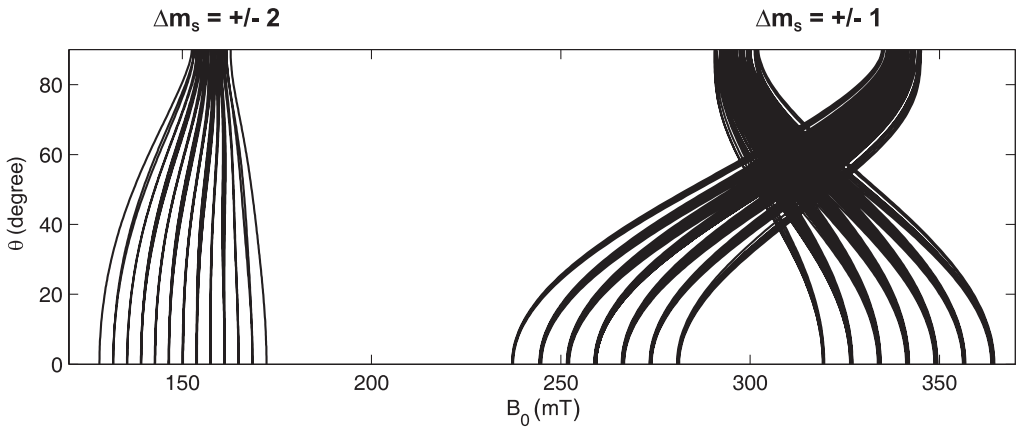

FIG. 7. Numerically simulated orientation dependence of allowed ($\Delta m_S = \pm 1$) and forbidden ($\Delta m_S = \pm 2$) transitions for the Cu^{2+}-Cu^{2+} dimeric center invoking the spin-Hamiltonian parameters given in Table I. The *half-field* resonances show a markedly reduced orientation dependence as compared to the allowed transitions.

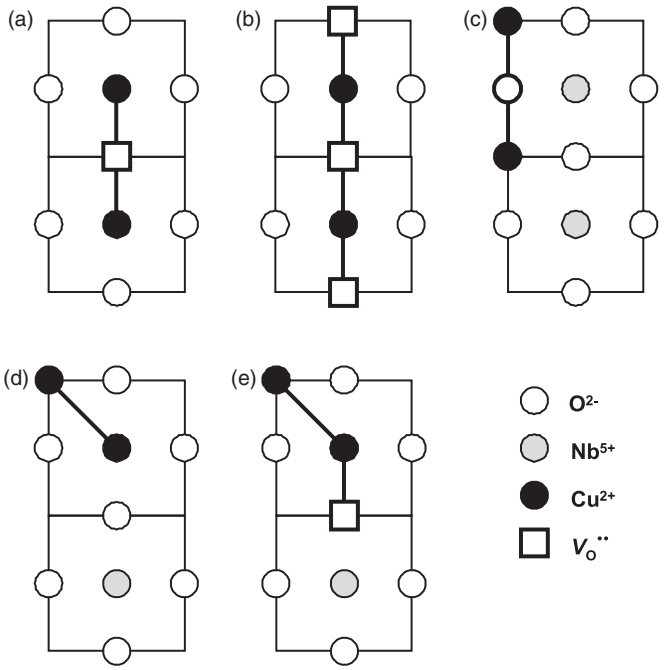

FIG. 8. Schematic illustration of conceivable arrangements for the Cu^{2+}-Cu^{2+} dimeric center in a pseudocubic $NaNbO_3$ unit cell. (a) $(Cu'''_{Nb} - V_O^{\bullet\bullet} - Cu'''_{Nb})''''$. (b) $(V_O^{\bullet\bullet} - Cu'''_{Nb} - V_O^{\bullet\bullet} - Cu'''_{Nb} - V_O^{\bullet\bullet})^{\times}$. (c) $(Cu^{\bullet}_{Na} - Cu^{\bullet}_{Na})^{\bullet\bullet}$. (d) $(Cu^{\bullet}_{Na} - Cu'''_{Nb})''$. (e) $(Cu^{\bullet}_{Na} - V_O^{\bullet\bullet} - Cu'''_{Nb})^{\times}$. Open circle: oxygen; open square: oxygen vacancy; gray circle: niobium; and black circle: copper.

would result in the formation of a double-positive charged $(Cu^{\bullet}_{Na} - Cu^{\bullet}_{Na})^{\bullet\bullet}$ defect complex [cf. Fig. 8(c)]. This situation with an incorporation of Cu^{2+} at the perovskite *A* site, however, is rather unlikely to be accomplished for a compound being synthesized with 2.0 mol% sodium excess.

An alternative scenario would be the incorporation of Cu^{2+} at the Nb site, which would then form a fourfold-negative charged $(Cu'''_{Nb} - V_O^{\bullet\bullet} - Cu'''_{Nb})''''$ defect complex [cf. Fig. 8(a)]. Because of the large charge mismatch of this defect complex, it seems rather unfavorable for the lattice to tolerate such defects. This problem can be circumvented if two oxygen vacancies are additionally associated, such that an electrically neutral $(V_O^{\bullet\bullet} - Cu'''_{Nb} - V_O^{\bullet\bullet} - Cu'''_{Nb} - V_O^{\bullet\bullet})^{\times}$ defect complex is generated [cf. Fig. 8(b)]. Owing to the experimentally observed axial symmetry of the center, the Cu'''_{Nb} and $V_O^{\bullet\bullet}$ are arranged along one orientation. However, all three defect-structure models considered so far involve an interspin distance between the two Cu^{2+} centers equal to the $NaNbO_3$ lattice constant $r_{12} \approx 4$ Å, which surpasses the experimentally determined value.

A model that results in a smaller interspin distance is provided by the *amphoteric* incorporation of the two adjacent Cu^{2+} centers at both cation sites, thus leading to a double-negative charged $(Cu^{\bullet}_{Na} - Cu'''_{Nb})''$ defect complex [cf. Fig. 8(d)]. By taking into account the $NaNbO_3$ lattice constant (≈4 Å) and neglecting any distortion from cubic symmetry, the corresponding interspin distance amounts to $r_{12} \approx 2\sqrt{3}$ Å = 3.46 Å, which fits to the spectroscopically determined value within the experimental error. Possibly, this defect complex could also involve an oxygen vacancy $(Cu^{\bullet}_{Na} - V_O^{\bullet\bullet} - Cu'''_{Nb})^{\times}$, thus being charge neutral [cf. Fig. 8(e)]. Because this defect has lower than axial site symmetry at the Cu^{2+} site, there is a discrepancy with the experimentally determined axial site symmetry.

More generally, when discussing all hitherto considered dimeric models illustrated in Fig. 8 at first view, it seems unlikely that an incorporation of the Cu^{2+} simultaneously on *A* and *B* sites always occurs in nearest-neighbor unit cells with a well-defined Cu^{2+}-Cu^{2+} interspin distance instead of a broad distribution of distances between the Cu^{2+} centers. However, recently, an analogous defect structure has been proposed for Mn-doped $BaTiO_3$ ceramics, involving the formation of a $(Mn'_{Ti} - V_O^{\bullet\bullet} - Mn'_{Ti})^{\times}$ defect complex.[61] More specific, the existence of ferromagnetically coupled Cu^{2+}-Cu^{2+} centers has recently been reported in a copper-doped $KTaO_3$ single crystal.[62] In this work, the Cu^{2+}-Cu^{2+} dimeric centers were suggested being arranged in a linear complex with three oxygen vacancies. Moreover, a reduced Cu^{2+}-Cu^{2+} interspin distance as compared to the lattice constant of $KTaO_3$ has been explained by spin ordering. The here discussed formation of dimeric Cu^{2+}-Cu^{2+} defect centers incorporated into the $NaNbO_3$ lattice in terms of a *linear* $(V_O^{\bullet\bullet} - Cu'''_{Nb} - V_O^{\bullet\bullet} - Cu'''_{Nb} - V_O^{\bullet\bullet})^{\times}$ defect complex thus provides a possible scenario.

As a further scenario, the formation of secondary phases containing the Cu^{2+}-Cu^{2+} dimeric center will be discussed. In that respect, the driving force for the formation of secondary phases can be rationalized as being due to the Na excess lying above the solubility limit.[17] The Cu^{2+}-dopant concentration of 0.25 mol%, however, is expected to be below the solubility limit, which, for most other perovskite compounds, is below about 1.0 mol%.[63–65]

With respect to the formation of secondary phases, first the Na_3NbO_4 secondary phase[66,67] is considered that has been identified in the XRD patterns for the 2.0 mol% sodium-excess compound. The Nb-Nb distance in the corresponding crystal structure has been determined to 3.38 Å.[66] Assuming that the Cu^{2+} replace the Nb^{5+} ions, this distance is within the experimentally determined interval for the Cu^{2+}-Cu^{2+} dimer. Similar to the above-discussed situation for sodium niobate, charge compensation in the Na_3NbO_4 secondary phase is expected to be accomplished by the formation of oxygen vacancies.

In order to test this hypothesis, a set of 0.25 mol% Cu^{2+}-doped $NaNbO_3$ ceramics with 2.0 mol% sodium excess has been prepared at varying sintering temperatures T_{sint} between 937 °C and 1150 °C. Obviously, the amount of secondary phase formed strongly depends on T_{sint} as illustrated in Fig. 9(a); with decreasing sintering temperature, the amount of Na_3NbO_4 markedly increases. The corresponding EPR spectra are shown in Fig. 9(b). Here, the intensity of the Cu^{2+}-Cu^{2+} dimeric center remains invariant on variation of T_{sint}, but, on the other hand, pronounced variations in the region at 320–325 mT can be observed (marked with an asterisk). The correlation of x-ray and EPR results necessitates a quantitative comparison of the amounts of secondary phase and Cu^{2+}-Cu^{2+} dimer formed. If the amount of Cu^{2+}-Cu^{2+} dimers incorporated into the Na_3NbO_4 would increase with larger fraction of secondary phase, a higher intensity of the EPR signal would be expected for the ceramics sintered at

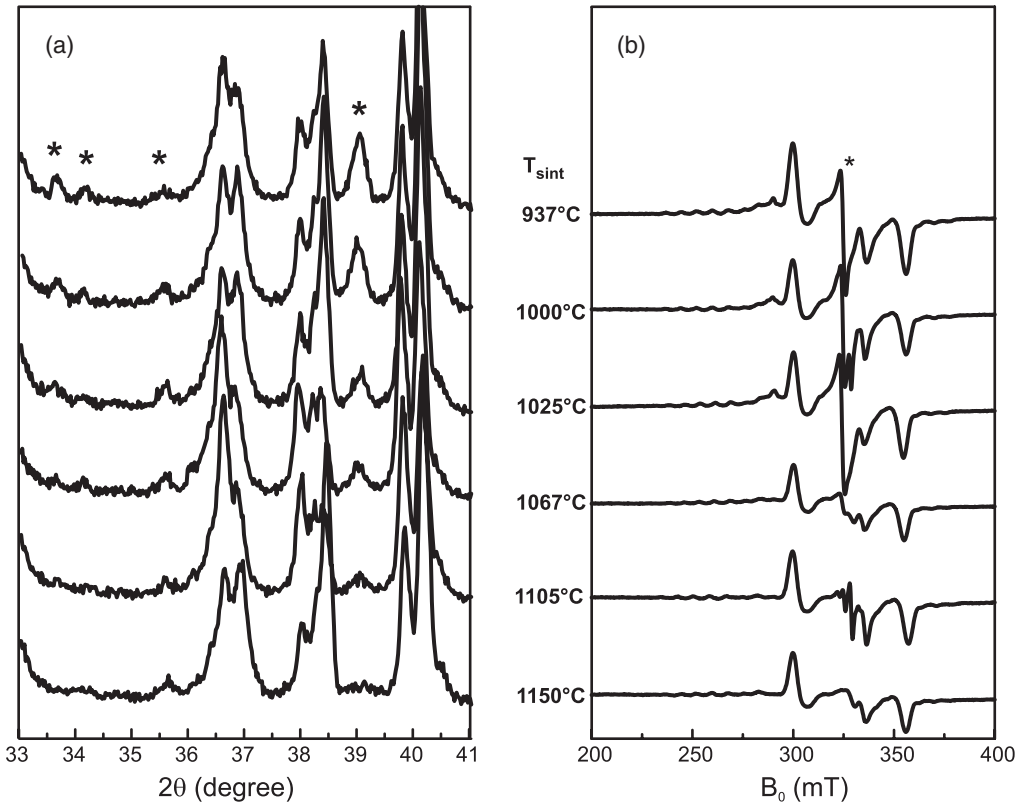

FIG. 9. Impact of sintering temperature T_{sint} on the development of Na_3NbO_4 secondary phase for 2.0 mol% Na-excess CuO-doped $NaNbO_3$. (a) section of XRD patterns relevant for the Na_3NbO_4 secondary phase. (b) *X*-band EPR spectra. The sintering temperatures are given above the spectra. The diffraction peaks and the EPR resonances owing to the secondary phase are marked by asterisks. The diffraction intensities of the x-ray patterns are normalized to the background.

lower temperature. However, if the amount of Na_3NbO_4 in the ceramics sintered at higher temperature is large enough to accommodate almost all available Cu^{2+} in the form of dimers, an increase in the Na_3NbO_4 phase content in the ceramics sintered at lower temperature will not show an increased EPR signal intensity of the Cu^{2+}-Cu^{2+} dimeric center because no additional Cu^{2+} is available. Accordingly, the observed results are not conclusive to distinguish between the Cu^{2+}-Cu^{2+} dimeric center being either incorporated into the $NaNbO_3$ lattice or into the Na_3NbO_4 secondary phase.

The spectral part that strongly depends on the sintering temperature and, hence, is assigned to Cu^{2+} defects in the Na_3NbO_4 secondary phase can also be numerically simulated (not shown) by involving an $S = 1$ state. This can either be due to trivalent copper (Cu^{3+}, $3d^8$) or another Cu^{2+}-Cu^{2+} dimeric center with considerably smaller fine structure and, thus, larger interspin distance. However, owing to extensive *g* and *A* strain, the spectral resolution is not sufficient to analyze this center in more detail.

Alternatively, the Cu^{2+}-Cu^{2+} dimeric center could be part of a $Na_xCu_yO_z$ secondary phase that intrinsically contains copper[68] with a concentration below the detection limit for XRD, but certainly above the one for EPR, which can be estimated between 10^0–10^{-9} mol%. Various $Na_xCu_yO_z$ phases have recently been studied.[69] However, in these compounds, strong magnetic interactions between the copper centers are present, which typically are orders of magnitude larger than the hyperfine interaction observed here. Correspondingly, EPR spectra of these compounds will be characteristic of broad and featureless resonances at *X*-band frequency, which differs from the here observed spectra exhibiting a well-resolved hyperfine septet pattern (cf. Fig. 2).

V. SUMMARY

In summary, the interplay between aliovalent CuO doping and nonstoichiometry on the defect structure and formation of secondary phases of antiferroelectric $NaNbO_3$ ceramics has been investigated by EPR and DFT. The results obtained show for stoichiometric 0.25 mol% CuO-doped $NaNbO_3$, as well as for 2.0 mol% Nb-excess sodium niobate, the incorporation of the Cu^{2+} functional centers at the Nb site (Cu'''_{Nb}). In the stoichiometric compound Cu^{2+}:$NaNbO_3$, two kinds of mutually compensating defect complexes ($Cu'''_{Nb} - V_O^{\bullet\bullet})'$ and ($V_O^{\bullet\bullet} - Cu'''_{Nb} - V_O^{\bullet\bullet})^{\bullet}$ are formed. With 2.0 mol% Nb excess, the amount of the dimeric ($Cu'''_{Nb} - V_O^{\bullet\bullet})'$ is decreasing as compared to the trimeric ($V_O^{\bullet\bullet} - Cu'''_{Nb} - V_O^{\bullet\bullet})^{\bullet}$ defect complex. Owing to the high structural tolerance of the material to nonstoichiometry, in this case, charge compensation is accomplished by the formation of sodium vacancies.

In contrast, for 2.0 mol% Na-excess sodium niobate compounds, a secondary phase (Na_3NbO_4) has been detected by XRD, and only part of the Cu^{2+} forms defect complexes in

analogy to the situation for the stoichiometric and Nb-excess $NaNbO_3$ compounds. Under the influence of sodium excess and the Na_3NbO_4 secondary phase, the major part of the Cu^{2+} tends to be present in a fundamentally different fashion by forming Cu^{2+}-Cu^{2+} dimeric centers. A definite assignment of this new center was not possible so far. If the dimeric center is incorporated to the Na_3NbO_4 secondary phase, the lack of variation in EPR intensity of this center with changes in the amount of Na_3NbO_4 secondary phase in the ceramic has to be further analyzed. If the dimeric centers are formed by Cu^{2+} substitution within the $NaNbO_3$ lattice, the challenges for future work are to investigate the reasons for nonaxial-symmetric arrangements in the case of neighboring amphoteric substitution and for reduced interspin distances between the Cu^{2+} ions in the case of the linear arrangement including oxygen vacancies.

ACKNOWLEDGMENTS

This research was financially supported by the DFG through Projects No. EI 498/1-2, No. EL 155/21-2, and No. HO 1165/14-2. E.E., P.J., and R.E. are very grateful for many helpful discussions with E. Erdem.

*r.eichel@physchem.uni-freiburg.de

[1] G. Shirane, R. Newnham, and R. Pepinsky, Phys. Rev. **96**, 581 (1954).
[2] A. M. Glazer and H. D. Megaw, Acta Crystallogr., Sect. A: Cryst. Phys., Diffr., Theor. Gen. Crystallogr. **29**, 489 (1973).
[3] J. Koruza, J. Tellier, B. Malic, V. Bobnar, and M. Kosec, J. Appl. Phys. **108**, 113509 (2010).
[4] M. D. Maeder, D. Damjanovic, and N. Setter, J. Electroceram. **13**, 385 (2004).
[5] T. R. Shrout and S. J. Zhang, J. Electroceram. **19**, 113 (2007).
[6] J. Rödel, W. Jo, K. T. P. Seifert, E. M. Anton, T. Granzow, and D. Damjanovic, J. Am. Ceram. Soc. **92**, 1153 (2009).
[7] R.-A. Eichel and H. Kungl, Funct. Mater. Lett. **3**, 1 (2010).
[8] B. Malic, D. Jenko, J. Bernard, J. Cilensek, and M. Kosec, Mater. Res. Soc. Symp. Proc. **755**, 83 (2003).
[9] M. Matsubara, T. Yamaguchi, K. Kikuta, and S. Hirano, Jpn. J. Appl. Phys. **43**, 7159 (2004).
[10] D. Lin, K. W. Kwok, and H. L. W. Chan, J. Phys. D: Appl. Phys. **41**, 045401 (2008).
[11] C. W. Ahn, M. Karmarkar, D. Viehland, D. H. Kang, K. S. Bae, and S. Priya, Ferroelectr., Lett. Sect. **35**, 66 (2008).
[12] Y. G. Lv, C. L. Wang, J. L. Zhang, M. L. Zhao, M. K. Li, and H. C. Wang, Mater. Lett. **62**, 3425 (2008).
[13] F. Azough, M. Wegrzyn, R. Freer, S. Sharma, and D. A. Hall, J. Eur. Ceram. Soc. **31**, 569 (2011).
[14] S. Körbel, P. Marton, and C. Elsässer, Phys. Rev. B **81**, 174115 (2010).
[15] R.-A. Eichel, E. Erünal, M. D. Drahus, D. M. Smyth, J. van Tol, J. Acker, H. Kungl, and M. J. Hoffmann, PhysChemChemPhys **11**, 8698 (2009).
[16] E. Erünal, R.-A. Eichel, S. Körbel, C. Elsässer, J. Acker, H. Kungl, and M. J. Hoffmann, Funct. Mater. Lett. **3**, 19 (2010).
[17] D. M. Smyth, *The Defect Chemistry of Metal Oxides* (Oxford University Press, New York, 2000).
[18] J. Acker, H. Kungl, and M. J. Hoffmann, J. Am. Ceram. Soc. **93**, 1270 (2010).
[19] R.-A. Eichel, PhysChemChemPhys **13**, 368 (2011).
[20] S. Körbel and C. Elsässer, Phys. Rev. B **84**, 014109 (2011).
[21] C. Van de Walle and J. Neugebauer, J. Appl. Phys. **95**, 3851 (2004).
[22] K. Reuter and M. Scheffler, Phys. Rev. B **65**, 035406 (2001).
[23] A. Shigemi and T. Wada, Jpn. J. Appl. Phys. **43**, 6793 (2004).
[24] C. Elsässer, N. Takeuchi, K. Ho, C. Chan, P. Braun, and M. Fähnle, J. Phys.: Condens. Matter **2**, 4371 (1990).
[25] K. Ho, C. Elsässer, C. Chan, and M. Fähnle, J. Phys.: Condens. Matter **4**, 5189 (1992).
[26] B. Meyer, K. Hummler, C. Elsässer, and M. Fähnle, J. Phys.: Condens. Matter **7**, 9201 (1995).
[27] F. Lechermann, F. Welsch, C. Elsässer, C. Ederer, M. Fähnle, J. M. Sanchez, and B. Meyer, Phys. Rev. B **65**, 132104 (2002).
[28] B. Meyer, F. Lechermann, C. Elsässer, and M. Fähnle (unpublished).
[29] D. Vanderbilt, Phys. Rev. B **32**, 8412 (1985).
[30] J. P. Perdew and A. Zunger, Phys. Rev. B **23**, 5048 (1981).
[31] A. Abragam and B. Bleaney, *Electron Paramagnetic Resonance of Transition Ions* (Clarendon, Oxford, 1970).
[32] J. R. Pilbrow, *Transition Ion Electron Paramagnetic Resonance* (Clarendon, Oxford, 1990).
[33] A. Bencini and D. Gatteschi, *EPR of Exchange-Coupled Systems* (Springer, Heidelberg, 1990).
[34] R.-A. Eichel, M. D. Drahus, P. Jakes, E. Erünal, E. Erdem, S. K. S. Parashar, H. Kungl, and M. J. Hoffmann, Mol. Phys. **107**, 1981 (2009).
[35] O. Bidault, M. Actis, and M. Maglione, Solid State Commun. **95**, 845 (1995).
[36] D. J. Keeble, Z. Li, and M. Harmatz, J. Phys. Chem. Solids **57**, 1513 (1996).
[37] W. L. Warren, B. A. Tuttle, F. C. Rong, G. J. Gerardi, and E. H. Poindexter, J. Am. Ceram. Soc. **80**, 680 (1997).
[38] Z. Bryknar, I. P. Bykov, M. D. Glinchuk, V. V. Laguta, Y. L. Maximenko, Z. Potucek, L. Jastrabik, and H. J. Schulz, Appl. Phys. A: Mater. Sci. Process. **66**, 555 (1998).
[39] H. T. Langhammer, T. Müller, R. Böttcher, and H. P. Abicht, Solid State Sci. **5**, 965 (2003).
[40] R.-A. Eichel, H. Kungl, and M. J. Hoffmann, J. Appl. Phys. **95**, 8092 (2004).
[41] R.-A. Eichel, K.-P. Dinse, H. Kungl, M. J. Hoffmann, A. Ozarowski, J. van Tol, and L. C. Brunel, Appl. Phys. A: Mater. Sci. Process. **80**, 51 (2005).
[42] N. M. Hagh, K. Kerman, B. Jadidian, and A. Safari, J. Eur. Ceram. Soc. **29**, 2325 (2009).
[43] S. Stoll and A. Schweiger, J. Magn. Reson. **178**, 42 (2006).
[44] F. A. Kröger and H. J. Vink, in *Solid State Physics*, Vol. 3, edited by F. Seitz and D. Turnbull, (Academic Press, New York and London, 1956), pp. 307–435.
[45] K. A. Müller, W. Berlinger, and J. Albers, Phys. Rev. B **32**, 5837 (1985).

[46]H. Meštrić, R.-A. Eichel, T. Kloss, K.-P. Dinse, So. Laubach, St. Laubach, P. C. Schmidt, K. A. Schönau, M. Knapp, and H. Ehrenberg, Phys. Rev. B **71**, 134109 (2005).
[47]E. Erdem, P. Jakes, S. K. S. Parashar, K. Kiraz, M. Somer, A. Rüdiger, and R.-A. Eichel, J. Phys.: Condens. Matter **22**, 345901 (2010).
[48]P. Jakes, E. Erdem, R.-A. Eichel, L. Jin, and D. Damjanovic, Appl. Phys. Lett. **98**, 072907 (2011).
[49]Rudiger-A. Eichel, P. Erhart, P. Träskelin, K. Albe, H. Kungl, and M. J. Hoffmann, Phys. Rev. Lett. **100**, 095504 (2008).
[50]A. S. Nowick and B. S. Berry, *Anelastic Relaxation in Crystalline Solids* (Academic, New York, 1972).
[51]P. V. Lambeck and G. H. Jonker, Ferroelectrics **22**, 729 (1978).
[52]G. Arlt and H. Neumann, Ferroelectrics **87**, 109 (1988).
[53]L. A. Reznichenko, L. A. Shilkina, O. N. Razumovskaya, I. V. Pozdnyakova, E. M. Kuznetsova, and S. I. Dudkina, Tech. Phys. **47**, 325 (2002).
[54]A. Shigemi and T. Wada, Jpn. J. Appl. Phys. **43**, 6793 (2004).
[55]N. H. Chan and D. M. Smyth, J. Am. Ceram. Soc. **67**, 285 (1984).
[56]J. G. M. van Rens and E. de Boer, Chem. Phys. Lett. **31**, 377 (1975).
[57]S. A. Altshuler, R. Kirmse, and B. V. Solovev, J. Phys. C: Solid State Phys. **8**, 1907 (1975).
[58]H. Yokoi and M. Chikira, J. Am. Chem. Soc. **97**, 3975 (1975).
[59]F. A. Yang, C. W. Guo, Y. J. Chen, J. H. Chen, S. S. Wang, J. Y. Tung, L. P. Hwang, and S. Elango, Inorg. Chem. **46**, 578 (2007).
[60]S. S. Eaton, K. M. More, B. M. Sawant, and G. R. Eaton, J. Am. Chem. Soc. **105**, 6560 (1983).
[61]T. Miki, A. Fujimoto, and S. Jida, J. Appl. Phys. **83**, 1592 (1998).
[62]D. V. Azamat, A. G. Badalyan, P. G. Baranov, P. P. Syrnikov, V. A. Trepakov, J. Rosa, and L. Jastrabik, Pis'ma Zh. E'ksp. Teor. Fiz. **69**, 890 (1999) [JETP Lett. **69**, 943 (1999)].
[63]H. J. Kleebe, S. Lauterbach, L. Silvestroni, H. Kungl, M. J. Hoffmann, E. Erdem, and R.-A. Eichel, Appl. Phys. Lett. **94**, 142901 (2009).
[64]E. Aksel, E. Erdem, P. Jakes, J. L. Jones, and R.-A. Eichel, Appl. Phys. Lett. **97**, 012903 (2010).
[65]M. D. Drahus, P. Jakes, E. Erdem, and R.-A. Eichel, Solid State Ionics **184**, 47 (2011).
[66]J. Darriet and J. Galy, Bull. Soc. Fr. Mineral. Cristallogr. **97**, 3 (1974).
[67]H. Näfe, R. Amin, and F. Aldinger, J. Am. Ceram. Soc. **90**, 3224 (2007); **90**, 3227 (2007).
[68]A. B. Kulakov, A. N. Maljuk, M. Sofin, C. T. Lin, B. Keimer, and M. Jansen, Solid State Chem. **177**, 3274 (2004).
[69]M. Sofin, Ph.D thesis, Max-Planck-Institut für Festkörperforschung, Stuttgart, 2003.